Conf-911109--4

UCRL-JC-107920
Preprint

Rec UCRL-JC--107920

DE92 002764

The Impact of Episodic Nonequilibrium Fracture-Matrix Flow on Repository Performance at the Potential Yucca Mountain Site

T. A. Buscheck, J. J. Nitao and D. A. Chesnut

Prepared for Submittal to Material
Research Society Conference
Strasbourg, France
November 4-7, 1991

Manuscript Date: October 1991
Publication Date: November 1991

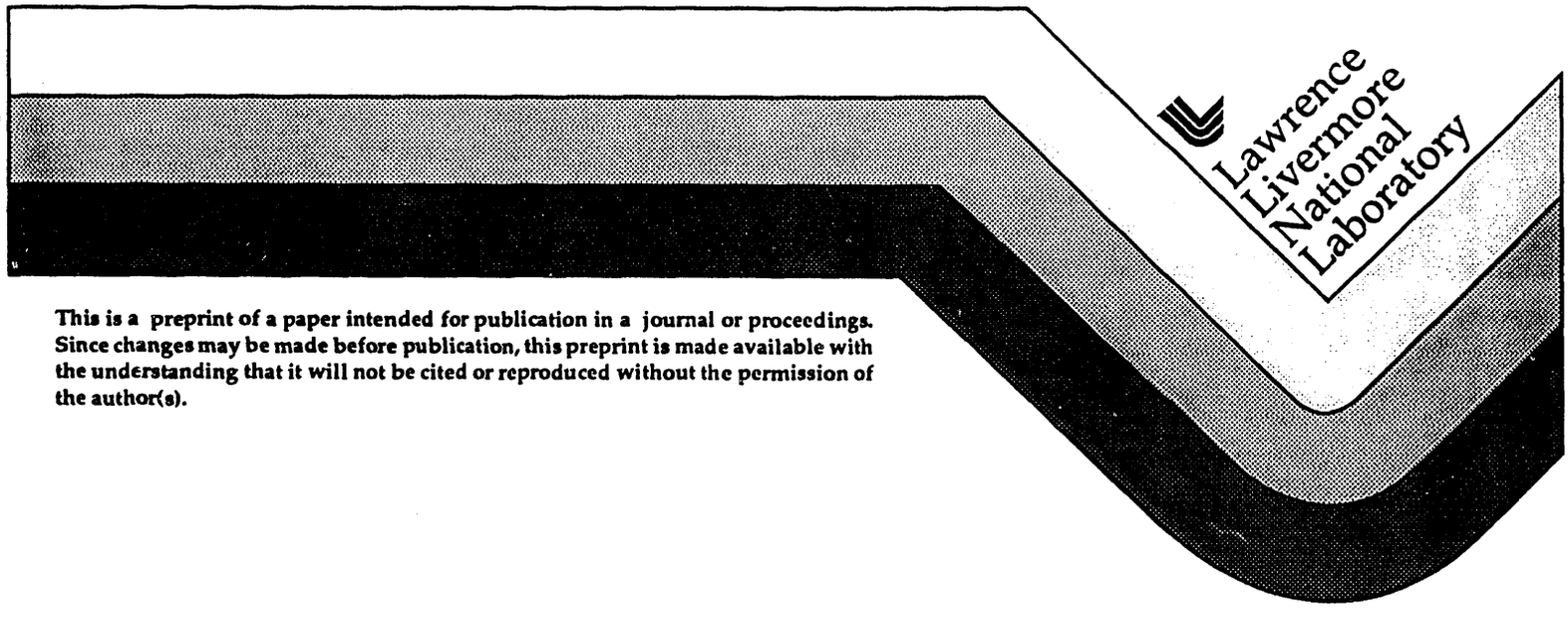

DISCLAIMER

THE IMPACT OF EPISODIC NONEQUILIBRIUM FRACTURE-MATRIX FLOW ON REPOSITORY PERFORMANCE AT THE POTENTIAL YUCCA MOUNTAIN SITE

Thomas A. Buscheck, John J. Nitao, and Dwayne A. Chesnut

Earth Sciences Department, Lawrence Livermore National Laboratory

P.O. Box 808, L-206, Livermore, CA 94550

(510) 423-9390, (510) 423-0297, (510) 423-5053

ABSTRACT

Adequate representation of fracture-matrix interaction during episodic infiltration events is crucial in making valid hydrological predictions of repository performance at Yucca Mountain. Approximations have been applied to represent fracture-matrix flow interaction, including the Equivalent Continuum Model, which assumes capillary equilibrium between fractures and matrix, and the Fracture-Matrix Model, which accounts for nonequilibrium fracture-matrix flow. We analyze the impact of matrix imbibition on episodic nonequilibrium fracture-matrix flow and transport for the eight major hydrostratigraphic units in the unsaturated zone at Yucca Mountain.

INTRODUCTION

The Yucca Mountain Site Characterization Project of the U.S. Department of Energy (DOE) is investigating the suitability of the fractured, tuffaceous rocks occurring in the unsaturated zone at Yucca Mountain, Nevada, for nuclear waste storage. Adequate representation of fracture-matrix interaction during episodic infiltration events is crucial in making valid hydrological predictions of repository performance. Various approximations have been applied to represent fracture-matrix flow interaction. The Equivalent Continuum Model (ECM) is a zeroth order approximation [1] which assumes instantaneous capillary equilibrium between the fracture and matrix. The second order approximation [2,3,4] explicitly accounts for the fracture and matrix porosities using the Fracture-Matrix Model (FMM). The FMM work has involved numerical modeling using the V-TOUGH code [5], which is a modified version of the TOUGH code [6], as well as the development of analytical and semi-analytical models [7]. Recent calculations also used the NUFT (Nonisothermal Unsaturated Flow and Transport) code, which has recently been developed at LLNL. This report describes the modeling of nonequilibrium fracture-matrix flow in the unsaturated zone at Yucca Mountain. The relative impact of matrix imbibition is analyzed for the eight major hydrostratigraphic units. The implications of nonequilibrium fracture-matrix flow on radionuclide transport are also discussed.

Background and Available Data

The potential repository location is in Topopah Spring (TSw2) moderately to densely welded tuff, which is about 350 m below the ground surface and 225 m above the water table [8]. The matrix properties of the hydrostratigraphic units at Yucca Mountain are summarized in Table 1 [8].

Table 1
Yucca Mountain Tuff Matrix Properties [8]

Unit	Sample Code	Porosity	Permeability m^2	S_r	α $10^{-2}m^{-1}$	β
TCw	G4-1	0.08	9.7×10^{-19}	0.002	0.821	1.558
PTn	GU3-7	0.40	3.9×10^{-14}	0.100	1.500	6.872
TSw1	G4-6	0.11	1.9×10^{-18}	0.080	0.567	1.798
TSw2	G4-6	0.11	1.9×10^{-18}	0.080	0.567	1.798
TSw3	GU3-11	0.07	1.5×10^{-19}	0.080	0.441	2.058
CHnv	GU3-14	0.46	2.7×10^{-14}	0.041	1.60	3.872
CHnz	G4-11	0.28	2.0×10^{-18}	0.110	0.308	1.602
PPw	G4-18	0.24	4.5×10^{-16}	0.066	1.41	2.639

w ≡ welded n ≡ nonwelded v ≡ vitric z ≡ zeolitized

With respect to the impact that matrix imbibition has on nonequilibrium fracture-matrix flow, the major hydrostratigraphic units at Yucca Mountain fall into two general categories: (1) the welded tuffs (TCw, TSw1, TSw2, and TSw3) and the nonwelded zeolitized unit (CHnz), all of which have low matrix permeability, k_m, and low-to-medium matrix porosity, ϕ_m, which are likely to promote fracture-dominated flow, and (2) nonwelded vitric units (PTn and CHnv) with high k_m and ϕ_m, which are more likely to promote matrix-dominated flow. Because of the small matrix pore size of all of the units, water in the matrix pores is held under high suction potential, causing the capillary fringe to extend from the water table to the ground surface (Fig. 1). Because of their low capillarity, most fractures will be drained of water under ambient conditions.

On the basis of one-dimensional steady-state ECM calculations, the observed range in saturation at the repository horizon [9] was found to correspond to a range in recharge flux of -0.005 to 0.05 mm/yr [10]. Figure 1 shows the vertical liquid saturation distribution from the water table to the ground surface, which corresponds to gravity-capillary equilibrium. Because of the relatively small capillarity of the high-k_m PTn and CHnv units, the high capillary suction potential of their neighboring units causes them to be drained to near-residual saturation. Figure 1 also includes recharge fluxes of 0.045 and 0.132 mm/yr, resulting in saturations at the repository horizon of 85 and 95 percent, respectively.

Saturation values obtained from the Reference Information Base (RIB) are also included in Fig. 1 [9]. While zero recharge flux results in a saturation of about 10 percent for the PTn and CHnv, the RIB reports mean saturation values of 61 and 91 percent, respectively. Obviously, significant recharge fluxes (i.e., much greater than those shown in Fig. 1) are able to reach the high-k_m units without affecting the saturation of the neighboring low-k_m units. Nonequilibrium fracture-matrix flow through the TCw, TSw1, TSw2, and TSw3 is a likely explanation for the inconsistency between the measured saturation data and the saturation profile predicted by the one-dimensional, steady-state ECM. Moreover, bomb-pulse ^{36}Cl measurements [11] are consistent with episodic nonequilibrium fracture flow from the ground surface to considerable depths. The discrepancy between the apparent near-zero recharge flux to the low-k_m units and the apparent large recharge flux to the high-k_m units can also be partially resolved by mechanisms that remove water from the vadose zone. These mechanisms may include vapor flow [12] as well as lateral liquid flow along high-k_m units such as the PTn and CHnv. The capacity of these mechanisms may be considerably in excess of what is currently required to provide a net zero flux at the repository horizon.

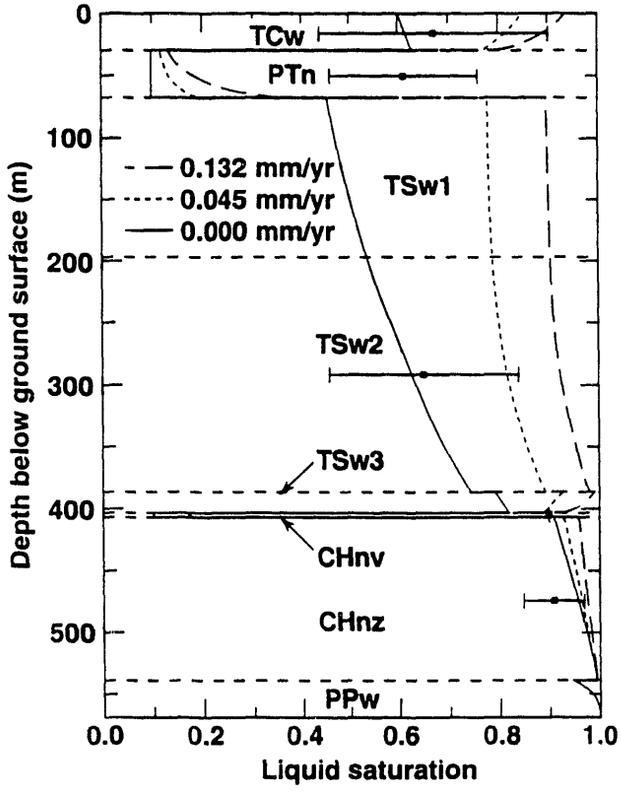

Fig. 1. ECM-calculated liquid saturation profiles for various steady-state, one-dimensional recharge fluxes compared with data from the Reference Information Base [9].

Matrix-Dominated vs Fracture-Dominated Flow

When the flux into a fracture is small enough, most of the water is imbibed by the matrix near the inlet before it moves a significant distance along the fracture [4]. The wetting front in the fracture lags behind the front in the matrix, and the wetting front speed is dominated by matrix properties. This condition corresponds to matrix-dominated flow. The ECM is satisfactory for this case.

Fracture-dominated flow occurs at higher fluxes. The wetting front in the fracture moves ahead of the front in the matrix, and matrix flow is primarily perpendicular to the fracture plane. Under these conditions, the speed of the wetting front in the fracture is governed by the competition between the driving forces in the fracture (gravity and fracture capillarity) and capillary imbibition into the matrix. Fracture-dominated flow can be classified into three physically interpretable flow periods [3,13], corresponding to the degree to which matrix interaction retards the speed of the wetting front in the fracture, with minimal retardation occurring during flow period I, intermediate retardation during flow period II, and maximal retardation during flow period III (Fig. 2). The ECM constrains flow to be either matrix-dominated or flow period III, thereby assuming the greatest possible degree of fracture flow retardation irrespective of whether it is physically valid to do so.

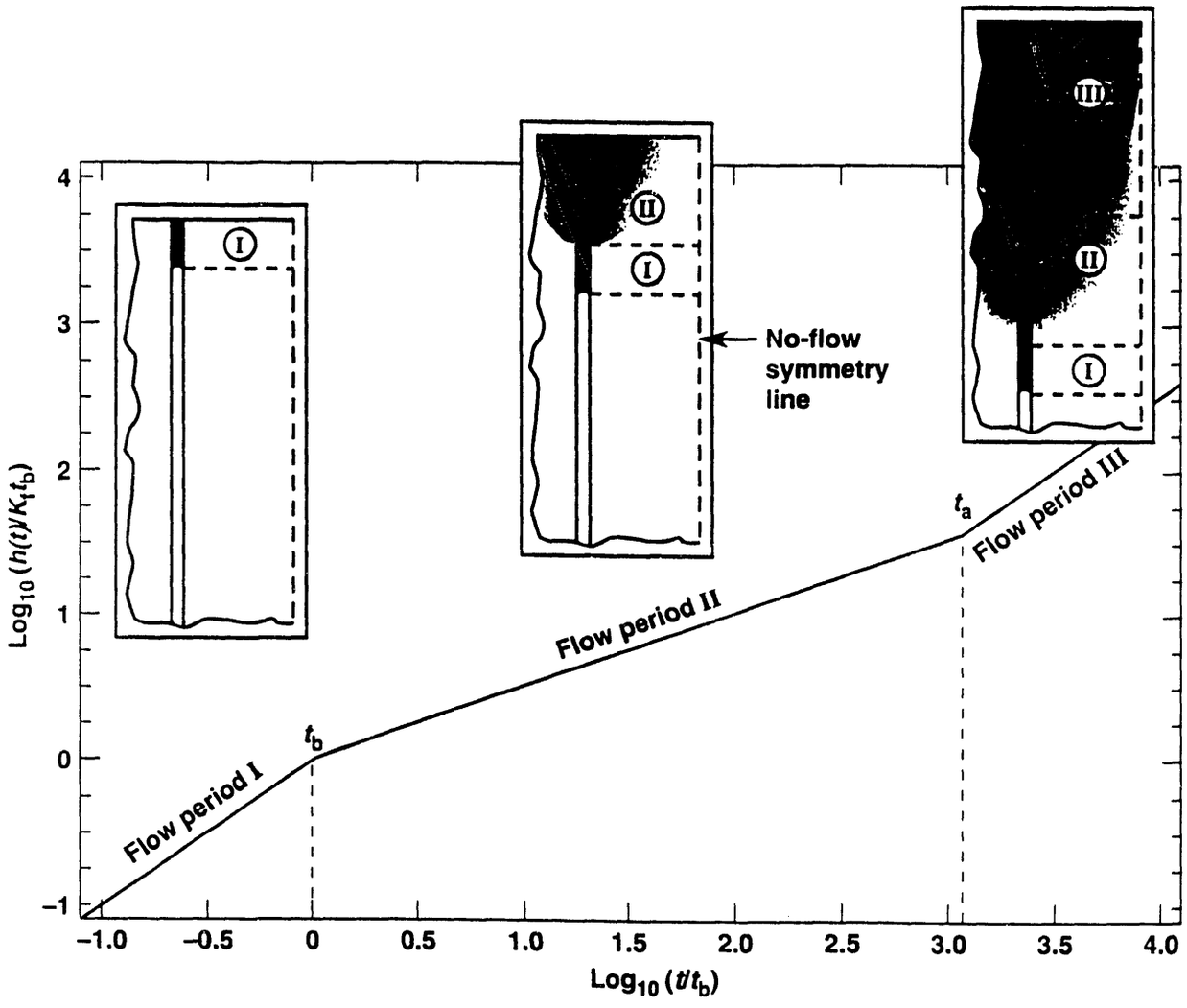

Fig. 2. The three major flow periods of fracture-dominated flow. The asymptotic dimensionless fracture front penetration, $h(t)/K_f t_b$, is plotted against dimensionless time, t/t_b, where $h(t)$ is the fracture penetration, K_f is the saturated hydraulic conductivity of the fracture, and t_b is the time required for one fracture pore volume to be imbibed by the matrix. The relationship between flow periods and flow regions is depicted in the insets.

The Importance of Spatial and Temporal Variability of Recharge Flux

Several analyses [3,4,10,13] indicate the need to account for the spatial variability and episodic nature of recharge flux. An important question is what sequencing of infiltration events gives rise to episodic behavior vs behavior that may be time-aggregated. Because of matrix imbibition, little additional penetration of the wetting front in a fracture occurs after a ponded source of water is removed [2]. For welded tuffs, the dimensionless liquid saturation, S_e, of the matrix wetting zone decays to within 10 percent of native saturation conditions within a few months. S_e is defined by

$$S_e = \frac{S - S_i}{1 - S_i}, \tag{1}$$

where S_i is the initial matrix saturation. For the CHnv it takes over 10 yr. For episodic infiltration events separated by a few days, the cumulative wetting front movement in the low-k_m units is nearly the same as would occur had all events occurred consecutively. For the CHnv, episodic events can be separated by a year without affecting the cumulative wetting front movement.

The high suction potential of the matrix will result in the waste package (WP) borehole being drained of water under low recharge flux. This phenomenon is the basis of one of the primary hydrological performance attributes of the WP emplacement configurations: a capillary barrier exists between the WP and the borehole wall, so no pore water should contact the WPs. As long as rock around the WP remains partially saturated and the capillary barrier is intact, there is no mechanism other than fracture flow to allow water to contact the WPs. Therefore, since fracture flow ceases soon after the removal of an infiltration source, the key consideration determining whether water will contact the WP is the intensity and duration of the maximum possible infiltration episode, i.e., an event or a group of events that effectively act as a single event.

Given that fracture flow along preferential flow paths provides the most likely means of transporting radionuclides to the water table, there are two major hydrological attributes of Yucca Mountain that will tend to physically retard the vertical movement of radionuclides. The first is the degree to which these paths are discontinuous. This consists of flow features that laterally divert or attenuate fracture flow. In addition to lateral attenuation due to matrix imbibition, flow branching from major fracture pathways into tributary fractures will have a lateral dispersive effect on fracture flow, enhancing the impact of matrix imbibition.

MODELING EPISODIC NONEQUILIBRIUM FRACTURE-MATRIX FLOW

We consider a two-dimensional system of vertical, parallel, uniformly spaced fractures extending continuously from the ground surface to the water table. Because of symmetry, we can consider an infinite periodic two-dimensional system extending from the no-flow boundary at the midplane of the fracture to the no-flow boundary at the midplane of the matrix block. Liquid enters the top of the fracture under a constant pressure due to ponding. FMM calculations [13] considered two suites of cases. In the first suite, the top of the fracture represents the floor of a drift at the repository. In the second suite, the top of the fracture represents either the ground surface or the base of the alluvium (e.g., within a wash or the streambed of an ephemeral stream).

Using the matrix property data listed in Table 1, we modeled the eight major hydrostratigraphic units in the unsaturated zone [10,13]. Note that k_m of all the units is reduced by a factor of 40 in order to account for an apparent capillary hysteresis effect [10,13]. Data on fracture properties in Yucca Mountain is sparse. For a range of fracture spacings listed in Table 2, the hydraulic aperture was calculated on the basis of the cubic law [10,14] and reported bulk permeability measurements [15,16]. FMM calculations [13] considered fracture apertures, b, of 10, 50, 100, 200, 400, and 1000 μm. The Environmental Assessment [17] reports from 15 to 40 fractures/m^3 for welded units and as

Table 2
Calculated Fracture Apertures Based on Reported Bulk Hydraulic Conductivities [15,16]

Assumed fracture spacing, B (m)	Fracture aperture, b (μm)
1.00	203 to 587
0.3	141 to 407
0.1	94 to 273
0.01	43 to 127

few as 1 fracture/m^3 for nonwelded units. Because many fractures will not lie along fracture pathways that are connected to an overlying source of water, the effective fracture spacing is likely to be much greater than the apparent fracture spacing. Fracture spacings, B, of 0.3, 3.0, 30, 100, and 400 m have also been modeled [13].

Episodic Flow Driven By Ponded Conditions at the Repository Horizon

Before conducting the episodic infiltration calculations, it was necessary to initialize the saturation and pressure fields in the model. For the reference case, a steady-state recharge flux of 0.045 mm/yr was used, resulting in a repository saturation of 85 percent (Fig. 1), which lies at the upper end of the range of measured saturations at this horizon [9]. The saturation at the water table is fixed at 100 percent. A ponded upper boundary is maintained at the repository horizon (at $p_e = 1$ atm, where p_e is the fracture entrance pressure), until the wetting front breaks through to the water table, located 225 m below the repository. Figure 3(a) is a contour plot of dimensionless liquid saturation, S_e [Eq. (1)], 2 h into this episodic event. The ECM predicts a very different saturation distribution for this case [Fig. 3(b)], with the wetting front only penetrating 0.56 m vertically after 2 h. The ECM assumes instantaneous mass transfer from the fracture to the entire initially unsaturated matrix porosity, resulting in maximal retardation of the wetting front in the fracture.

The impact of matrix flow on the wetting front movement is illustrated by comparing portions of the groundwater travel time, *GWTT*, for wetting front penetration through (1) the low-k_m TSw2 and TSw3, and (2) the high-k_m CHnv (column 2 of Table 3). For the reference case (b = 100 μm and B = 30 m), the low k_m of the TSw2 and TSw3 promotes fracture-dominated flow period I. Consequently, it takes only 4.5 h for the wetting front to penetrate those units. The high k_m of the CHnv promotes matrix-dominated flow for about 240 days. Because of the small thickness of the CHnv and the matrix imbibition flux decaying as $t^{-1/2}$, fracture-dominated flow period III is eventually established in the CHnv and the wetting front is able to reach the CHnz at t = 241 days. Even after the CHnv is penetrated, the large lateral matrix flow into this layer continues to retard the speed of the wetting front as it penetrates the CHnz and PPw, causing it to take an additional 49 days to

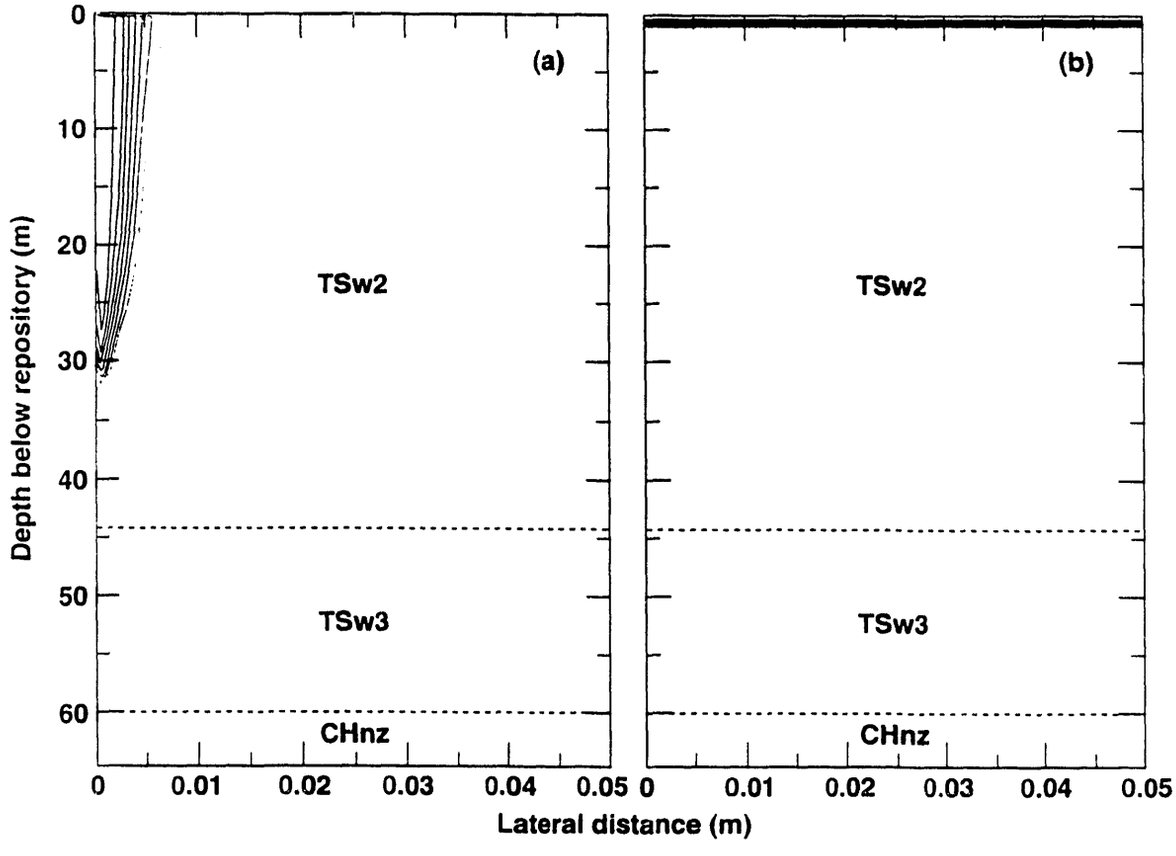

Fig. 3. Dimensionless liquid saturation, S_e, for a 100-μm fracture, a fracture spacing of 3.0 m, and ponded conditions at the repository horizon at t = 2 h. (a) FMM calculation. (b) ECM calculation

Table 3 b = 100 μm; B = 30 m				
	GWTT (FMM) (w/o matrix) (s)	*GWTT* (FMM) (w/ matrix) (s)	R_m (FMM)	R_m (ECM)
TSw2 & TSw3	7359.	1.62×10^4	2.2	4550.
CHnv	551.	2.08×10^7	3.87×10^4	1.37×10^5
CHnz & PPw	1.96×10^4	3.18×10^6	162.	3730.
TOTAL	2.76×10^4	2.45×10^7	887.	6620.

Table 4 b = 1000 μm; B = 3.0 m				
	GWTT (FMM) (w/o matrix) (s)	*GWTT* (FMM) (w/ matrix) (s)	R_m (FMM)	R_m (ECM)
TSw2 & TSw3	70.	70.	1.0	45.6
CHnv	5.5	30.	5.4	1372.
CHnz & PPw	200.	245.	1.2	37.5
TOTAL	276.	345.	1.3	66.1

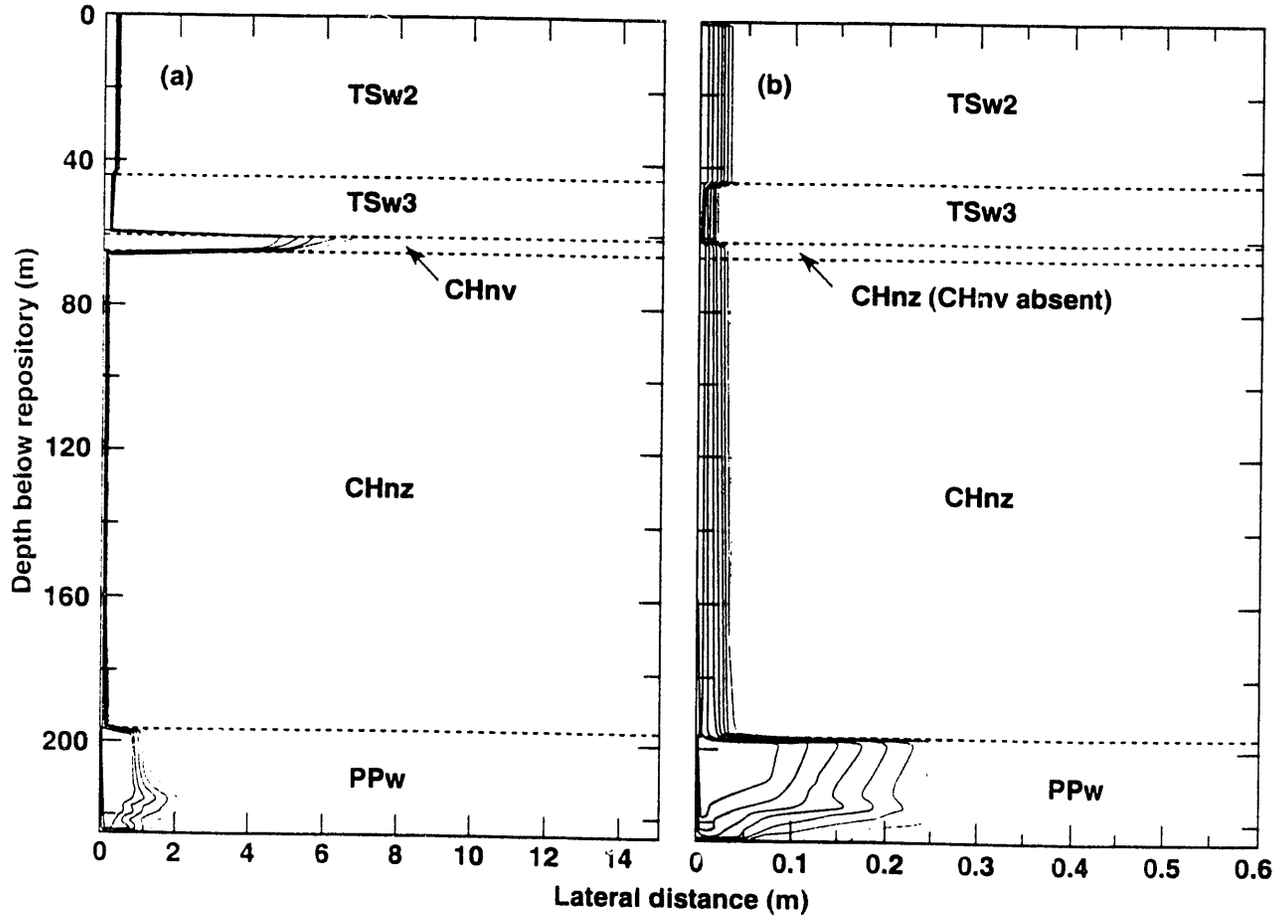

Fig. 4. FMM-calculated dimensionless liquid saturation, S_e, for a 100-μm fracture, a fracture spacing of 30 m, and ponded conditions at the repository horizon. (a) With the CHnv at t = 290 days, and (b) without the CHnv at t = 52 h. Note the different lateral scales.

reach the water table [Fig. 4(a)]. For b = 1000 μm (Table 4), the large fracture conductivity dominates flow, with flow period I persisting in all but the CHnv. where flow period II prevails. Notice that it only takes 70 s for the wetting front to reach the CHnv, another 30 s to penetrate the CHnv, and a total of only 345 s to reach the water table (Table 4).

Tables 3 and 4 illustrate the impact of matrix flow by comparing *GWTT* for the case of no matrix flow (column 1) with the case of fracture-matrix interaction (column 2). Column 3 lists the "retardation" ratio, R_m, defined as the ratio of the *GWTT* with matrix interaction to the *GWTT* without matrix interaction. In other words, R_m is the factor by which *GWTT* is delayed by virtue of matrix interaction. Column 4 lists R_m predicted by the ECM. Effectively, the ECM provides instantaneous matrix interaction over all of the matrix porosity lying between wetting fractures.

A three-dimensional map of the major hydrostratigraphic units at Yucca Mountain [18] indicates that the CHnv is not areally extensive over the repository block. Therefore, we repeated the episodic flow calculations for situations in which the CHnv is absent. For b = 100 μm and B = 30 m, the absence of the highly attenuating CHnv results in the wetting front taking only 52 h to reach the water table [Fig. 4(b)]. Obviously, the presence (or absence) of the high-k_m CHnv unit has a profound effect on fracture-matrix flow below the repository.

Episodic Flow Driven By Ponded Conditions at the Ground Surface

This section considers episodic fracture-matrix flow starting from the ground surface and going through the low-k_m TCw, the high-k_m PTn, and the low-k_m TSw1 and TSw2 (Table 1). A steady-state recharge flux of 0.045 mm/yr was once again used in the reference case (Fig. 1). Because of the small k_m of the TCw, it only takes 1.5 h for the wetting front in a 100-μm fracture to penetrate it and reach the PTn. In order to observe the lateral spread of the wetting zone in the PTn without the effect of interference with neighboring fractures, a large fracture spacing was modeled (B = 400 m). The large k_m of the PTn results in matrix-dominated flow for about 62 yr. Between t = 62 and 64 yr, flow in the PTn undergoes a transition to fracture-dominated flow period III, facilitating the penetration of the wetting front to the TSw1. Even after the PTn is penetrated, the propagation of the wetting front through the TSw1 and TSw2 continues to be dominated by matrix flow in the PTn. Consequently, it takes an additional 6 years for the wetting front to reach the repository horizon [Fig. 5(a)]. Note that gravity has also been contributing to lateral matrix flow in the PTn.

For a 1000-μm fracture, it takes only 30 s for the wetting front to penetrate the TCw. The high-k_m PTn then dominates flow for about 2200 s, after which there is a transition to fracture-dominated flow period III. The wetting front penetrates the PTn in about 2400 s, reaching the repository horizon [Fig. 5(b)] in 1 h.

Summary of Model Results: Implications for Site Suitability and Radionuclide Transport

Figure 6 summarizes the 100-μm fracture cases, which were driven by ponded conditions at either the ground surface or the repository. Notice that it takes about 100 to 10,000 times longer for a wetting front starting at the ground surface to reach the repository than for a wetting front starting at the repository to reach the water table. Apparently, Yucca Mountain's capacity to attenuate and retard liquid pulses (by virtue of matrix interaction) primarily resides above the repository.

As a liquid pulse moves down a fracture, it is continually losing water by imbibition into the adjoining matrix. If a pulse were intense enough to allow water to reach a failed WP, it could dissolve radionuclides and transport them toward the water table. Shortly after the end of the episodic event, liquid in the fracture would be totally imbibed by the matrix along with any dissolved radionuclides. Although subsequent pulses might transport "additional" radionuclides, their capability to further displace radionuclides imbibed by the matrix during earlier events will be limited. This limited capability to further vertically displace radionuclides stems from the fact that the matrix imbibition diffusivity of the low-k_m units is at least as great as the molecular or ionic diffusivities. Hence, advection by imbibition away from the fracture will tend to dominate molecular diffusion toward the fracture, limiting the re-entrainment of previously imbibed radionuclides by subsequent fracture pulses.

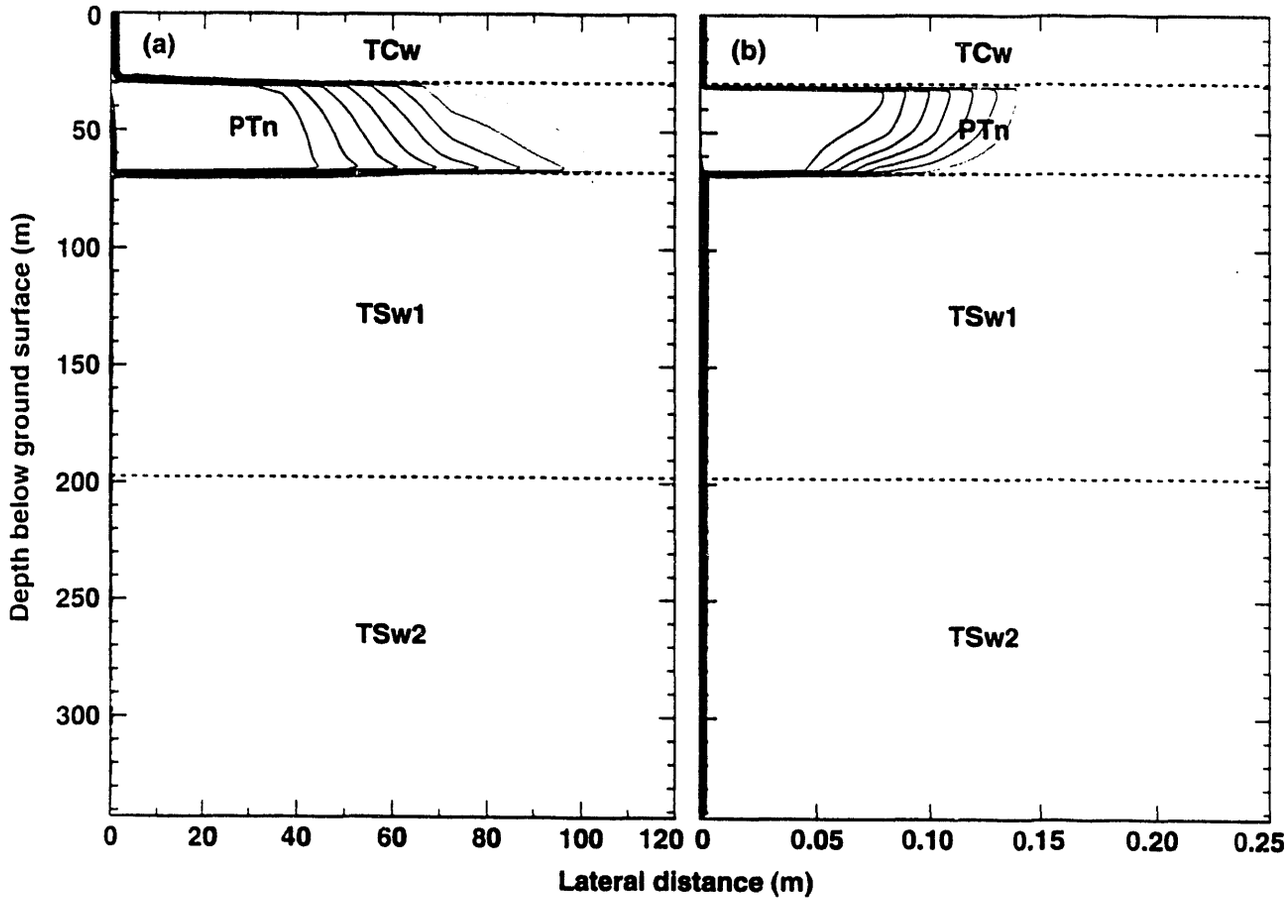

Fig. 5. FMM-calculated dimensionless liquid saturation, S_e, for ponded conditions at the ground surface and a fracture spacing of 400 m. (a) 100-μm fracture at t = 70 yr. (b) 1000-μm fracture at t = 1 h. Note the different lateral scales.

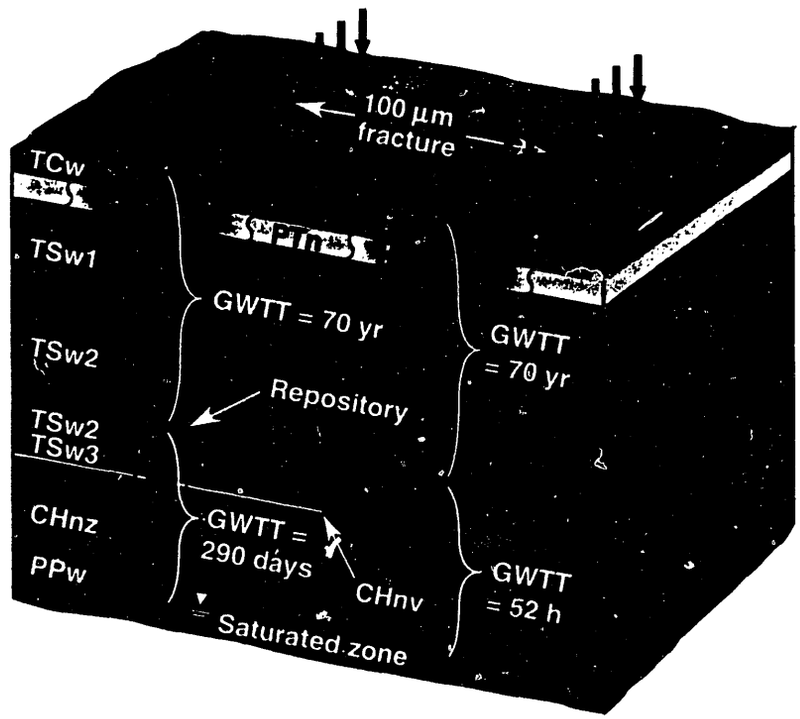

Fig. 6. Summary of FMM calculations of episodic nonequilibrium fracture-matrix flow for 100-μm fractures, with and without the CHnv.

CONCLUSIONS

Saturation measurements [9], "bomb-pulse" ^{36}Cl measurements [11], and the results of this modeling study are all consistent with episodic fracture flow from the ground surface to considerable depths. With respect to the impact that matrix imbibition has on nonequilibrium fracture-matrix flow, the major hydrostratigraphic units at Yucca Mountain fall into two general categories: (1) the low-k_m welded tuffs (TCw, TSw1, TSw2, and TSw3) and the low-k_m nonwelded zeolitized unit (CHnz), which are likely to promote fracture-dominated flow, and (2) the high-k_m nonwelded vitric units (PTn and CHnv), which are more likely to promote matrix-dominated flow. Nonequilibrium fracture-matrix flow can explain the discrepancy between the apparent near-zero recharge flux to the low-k_m units and the large recharge flux to the high-k_m units. The discrepancy can also be partially resolved by mechanisms that remove water from the vadose zone. These mechanisms may include vapor flow [12] as well as lateral liquid flow along high-k_m units such as the CHnv. For scenarios in which Yucca Mountain is not gradually saturating, key considerations in analyzing radionuclide transport are the intensity and duration of the maximum possible infiltration episode.

Acknowledgments

The authors acknowledge the review comments of Richard Knapp and editorial assistance of Jay Cherniak. This work was supported by the Nearfield Hydrology Task (WBS 1.2.2.2.2) of the Yucca Mountain Site Characterization Project. Work performed under the auspices of the U.S. Department of Energy by Lawrence Livermore National Laboratory under Contract W-7405-Eng-48.

References

1. Klavetter, E.A., and R.R. Peters, "A Continuum Model for Water Movement in an Unsaturated Fracture Rock Mass," Water Resources Research, Vol. 24, pp. 416-430 (1988).
2. Buscheck, T.A., and J.J. Nitao, "Estimates of the Width of the Wetting Zone Along a Fracture Subjected to an Episodic Infiltration Event in Variably Saturated, Densely Welded Tuff," UCID-21579, Lawrence Livermore National Laboratory, Livermore, CA (1988).
3. Nitao, J.J., and T.A. Buscheck, "On the Infiltration of a Liquid Front in an Unsaturated, Fractured Porous Medium," Proceedings American Nuclear Society Topical Meeting on Nuclear Waste Isolation in the Unsaturated Zone (Focus 89), Las Vegas, NV, Sept. 17-21 (1989).
4. Nitao, J.J., "Theory of Matrix and Fracture Flow Regimes in Unsaturated, Fractured Porous Media," UCRL-JC-104933, Lawrence Livermore National Laboratory, Livermore, CA (1991).
5. Nitao, J.J., "V-TOUGH - An Enhanced Version of the TOUGH Code for the Thermal and Hydrologic Simulation of Large-Scale Problems in Nuclear Waste Isolation," UCID-21954, Lawrence Livermore National Laboratory, Livermore, CA (1989).
6. Pruess, K. "TOUGH User's Guide," NUREG/CR-4645, Nuclear Regulatory Commission (1987).
7. Nitao, J.J., "On the Infiltration of a Liquid Front in an Unsaturated, Fractured Porous Media, Part II," UCID-21743, Lawrence Livermore National Laboratory, Livermore, CA (1989).
8. Klavetter, E.A., and R.R. Peters, "Estimation of Hydrologic Properties of an Unsaturated Fracture Rock Mass," SAND84-2642, Sandia National Laboratories, Albuquerque, NM (1986).
9. DOE (U.S. Dept of Energy), "Yucca Mountain Project Reference Information Base," YMP/CC-0002 (Version 04.002),Nevada Operations Office, Las Vegas, NV (1990).
10. Buscheck, T.A., and J.J. Nitao, "Nonequilibrium Fracture-Matrix Flow During Episodic Infiltration Events in Yucca Mountain," Proceedings of the Fifth NRC Workshop on Flow and Transport through Unsaturated Fractured Rock, Univ. of Arizona, Tuscon, AZ, Jan. 7-10, 1991. Also, UCRL-ID-108311, Lawrence Livermore National Laboratory, Livermore, CA (1991).
11. Norris, A.E., "The Use of Chlorine Isotope Measurements to Trace Water Movements at Yucca Mountain," Proceedings American Nuclear Society Topical Meeting on Nuclear Waste Isolation in the Unsaturated Zone (Focus 89), Las Vegas, NV, Sept. 17-21 (1989).
12. Thorstenson, D.C., E.P. Weeks, H. Haas, and J.C. Woodward, "Physical and Chemical Characteristics of Topographically Affected Airflow in an Open Borehole at Yucca Mountain, Nevada," Proceedings American Nuclear Society Topical Meeting on Nuclear Waste Isolation in the Unsaturated Zone (Focus 89), Las Vegas, NV, Sept 17-21, 1989.

13. Buscheck, T.A., and J.J. Nitao, "Impact of Episodic Nonequilibrium Fracture-Matrix Flow on Geological Repository Performance," UCRL-JC-106759, Lawrence Livermore National Laboratory, Livermore, CA (1991).

14. Witherspoon, P.A., J.S.Y. Wang, K. Iwai, and J.E. Gale, "Validity of Cubic Law for Fluid Flow in a Deformable Rock Fracture," Water Resources Research, Vol. 16, pp. 1016-1024 (1980).

15. Montazer, P., E.P. Weeks, F. Thamir, S.N. Yard, and P.B. Hofrichter, "Monitoring the Vadose Zone in Fractured Tuff, Yucca Mountain, Nevada," Characterization and Monitoring of the Vadose Zone, National Water Well Association Symposium, Denver, CO, Nov. 19-21, 1985.

16. Thordarson, W., "Geohydrologic Data and Test Results from Well J-13, Nevada Test Site, Nye County, Nevada," Water Resources Investigations Rep. 83-4171, U.S.G.S., Denver, CO (1983).

17. DOE (U.S. Dept of Energy) "Environmental Assessment: Yucca Mountain Site, Nevada Research and Development Area, Nevada, Volume II," DOE/RW-0073, 1986.

18. Ortiz, T.S., R.L. Williams, R.B. Nimick, B.C. Whittet, and D.L. South, "Three-Dimensional Model of Reference Thermal-Mechanical and Hydrological Stratigraphy at Yucca Mountain, Southern Nevada," SAND84-1076, Sandia National Laboratories, Albuquerque, NM (1985).

DATE
FILMED
12/19/91